Data-Driven TD3 Control of IM Considering Magnetic Saturation and Temperature Effect

Ugur Ufuk Korpe
Dept. of Electrical-Electronics Engineering
Kirsehir Ahi Evran University
Kirsehir, Turkey
ugur.korpe@ahievran.edu.tr

Mustafa Gokdag
Dept. of Electrical-Electronics Eng.
Industrial Electronics Lab. (KBU-IEL)
Karabuk University
Karabuk, Turkey
mgokdag@karabuk.edu.tr

Ozan Gulbudak
Dept. of Electrical-Electronics Eng.
Industrial Electronics Lab. (KBU-IEL)
Karabuk University
Karabuk, Turkey
ozangulbudak@karabuk.edu.tr

2024 6th Global Power, Energy and Communication Conference (GPECOM) | 979-8-3503-5108-8/24/$31.00 ©2024 IEEE | DOI: 10.1109/GPECOM61896.2024.10582723

***Abstract*— Induction machines (IM) are still widely used in the industry due to their advantages, such as low maintenance requirements and improved robustness. The field-oriented control (FOC), direct torque control (DTC), and model predictive control (MPC) techniques are used to control IM in high-performance control applications. The common disadvantage of these control techniques is that the control performances are negatively affected by changes in machine parameters, and machine parameters vary non-linearly depending on the magnetic saturation and temperature. To solve this negative affect, the control technique can be optimized by using a parameter estimation methods. Another solution to eliminate these negative effects is to design a reinforcement learning (RL)-based controller that regulates the control variables without the knowledge of machine parameters. In this study, IM speed control is performed using a twin-delayed deep deterministic policy gradient (TD3) agent. The dynamic and steady-state performance of the designed controller are compared with the traditional control techniques. Extensive simulation results have shown that the dynamic and steady-state performance of the designed controller is better than other control techniques.**

Keywords—Induction motor, parameter estimation, reinforcement learning, TD3 agent

I. INTRODUCTION

Nowadays, high-performance control of electric machines is becoming increasingly popular as these machines are used in transportation, industrial, and household applications. IMs are one of these machines and are still widely used in these applications due to their advantages, such as not having rare-earth magnets in their rotors, being robust, having lower maintenance requirements, and having cost-effective production [1], [2]. In order to achieve high-performance control of IM in the abovementioned applications, speed or torque control must performed with control techniques such as FOC, DTC, and MPC [3].

The two techniques have been used in high-performance control applications of IM since the late 20th century. One is FOC, and the other is DTC [4], [5]. FOC is a linear control strategy and uses linear controllers to generate reference voltages. The motor then generates reference voltages by switching the inverter using the space-vector pulse width modulation (SVPWM) or sine pulse width modulation (SPWM) technique. The system has a constant switching frequency, and therefore the steady-state performance of the system is good. However, the inner and outer controllers are cascaded, so the system is complex. The coefficients of these controllers are difficult to adjust. Also, these coefficients are adjusted using machine parameters, and these machine parameters vary depending on the magnetic saturation, temperature, and skin effect [6], [7]. Controller coefficients need to be readjusted due to changes in machine parameters. In DTC, switching vectors are selected and applied to the inverter using a predefined look-up-table (LUT) without using modulation block and inner linear controllers. The system has a fast dynamic response due to these features. However, due to the absence of the modulator block, the steady-state performance of the system is poor. Also, the dynamic models of the machine are used in the torque and flux estimators in DTC. These dynamic models consist of motor parameters that vary due to the magnetic saturation and temperature, as mentioned before [8], [9]. The machine parameters must be estimated to control the machine properly; these estimations must be used in torque and flux estimators. After the discovery of FOC and DTC technologies, research on non-linear controllers increased with innovations in digital signal processors (DSPs) technology in the early 21st century. One of these non-linear controllers is the finite-control set model predictive control (FCS-MPC) technique [10]. FCS-MPC utilizes the discrete-time dynamic model of the system to estimate the control variables for each feasible control input and evaluates the cost function. For drive system applications, the control variables are electromagnetic torque, rotor speed, and stator currents. The control input that gives the minimum cost value is selected and applied to the system [11]. FCS-MPC technique is a promising control technique for drive system applications due to fast dynamic response, simple implementation, ability to control multi-variables using a cost function, and inclusion of system non-linearities and constraints via the discrete-time dynamic model of the system [12]. However, the disadvantages of this technique are that due to the absence of the modulator block, the system has a variable switching frequency and, therefore, has a poor steady-state performance [13]. One solution to this problem is to decrease the sampling time of the system. However, this increases the mathematical burden on the DSP [14]. Another solution is to add a modulator block into the system. The control technique using this solution is known as modulated model predictive control (M^{2}PC). This technique is indeed improves the steady-state performance of the system compared to FCS-MPC [15], [16]. However, since the discrete-time dynamic equations are used in FCS-MPC and M^{2}PC techniques, the performance of these control techniques depends on the accuracy of the machine parameters as in FOC and DTC techniques. Ignoring these parameter changes adversely affects the performance of the control techniques. This may even result in the machine not being controlled [17], [18]. In order to solve the adverse effects of machine parameter changes on control performance, in the literature, there are parameter estimation methods in which the parameters of IM are estimated using model reference adaptive system (MRAS), recursive least squares (RLS), and extended Kalman filter (EKF) methods. The estimated machine parameters are then used to optimize the control technique [19], [20], [21]. Another solution is to use RL, one of the types of machine learning, as a control technique.

979-8-3503-5108-8/24/$31.00 ©2024 IEEE

RL-based methods solve the control problem in an entirely data-driven manner. The block diagram of RL and the drive system is given in Figure 1. In RL methods, agents, the learning process is performed using a so-called reward function. The agent interacts with the environment, that is, everything except the RL agent, and takes action to maximize the predefined reward function, according to the information the agent obtains from the environment. Then, the agent determines the optimal policy of the control technique based on the actions the agent performs [22]. The environment for the drive system application is the inverter and IM. The agent interacts with the environment using signals from the inverter and IM. In this study, the selected RL agent is TD3, which can give continuous action output [23]. In the literature, a study conducted in 2020 showed that the current control of permanent magnet synchronous motor (PMSM) can be achieved using an actor-critic-based RL agent [24]. In the study in 2021, torque control of PMSM is performed in the simulation environment using another RL agent, deep Q learning (DQN). The results are compared with the FCS-MPC-based controller, and it has been shown that the dynamic and steady-state performances of the designed controller with the DQN agent are better than the FCS-MPC-based controller [25]. In [26], the speed control of IM is performed with the TD3-based FOC. However, the TD3 agent does not replace the inner controllers; the outer controller replaces the agent. Thus, the agent is a *q*-axis reference current. In [27], four different controllers, TD3-based, deep deterministic policy gradient (DDPG), linear quadratic Gauss (LQG) based, and BP network-based, are designed, and the speed control of PMSM using these controllers is performed. Simulation results show that the TD3-based controller gives better results than other controllers in dynamic and steady-state.

In RL-based controllers, since the agent interacts with the environment in a data-driven manner using only the signals it receives from the environment, the controller is independent of machine parameters [28]. The agent performs control according to these parameter changes since the change of machine parameters will affect the signals the agent receives from the environment. In this study, IM speed control is performed using a TD3-based controller. Proportional-integral (PI) controller is chosen as the outer controller, and the TD3 agent is defined as the inner controller. It is assumed that the parameters of the IM vary depending on the magnetic saturation and temperature. According to this assumption, the dynamic and steady-state performance of the controller with the TD3 agent is compared with other control techniques, FOC, FCS-MPC, and M^{2}PC, through extensive simulations. The simulation results have shown that the dynamic and steady-state performance of the TD3-based controller is robust against parameter changes depending on magnetic saturation and temperature. In addition, it has been shown that the dynamic and steady-state performance of the designed controller gives better results than other control techniques. The first part of this study presents a literature review of IM and the control methods. In the second part, mathematical expressions of the environment, which consist of the inverter and IM, are given. In the third part, mathematical expressions of the TD3 agent are presented. The fourth section shows the simulation results of the control with the TD3 agent and discusses the comparison results of this control with FOC, FCS-MPC, and M^{2}PC.

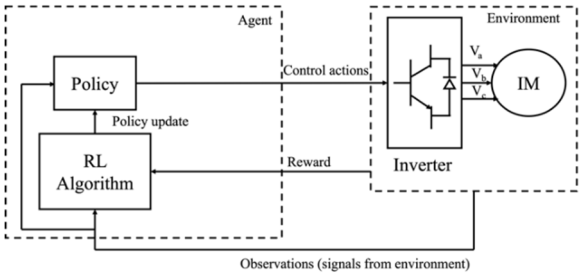

Fig. 1. The block diagram of RL

II. SYSTEM MODEL

A. Voltage-source inverter model

This section gives mathematical expressions of the environment in which the agent interacts. For this reason, the three-phase two-level voltage source inverter (VSI), whose circuit schematic is shown in Figure 2, is used as a power converter in the system. The VSI is assumed to be ideal and in a balanced load state. The phase-to-neutral voltages of phases *A,B,C*, respectively, of the inverter are given in (1) [29].

$$\begin{bmatrix} V_{An} \\ V_{Bn} \\ V_{Cn} \end{bmatrix} = \frac{V_{DC}}{3} \begin{bmatrix} 2 & -1 & -1 \\ -1 & 2 & -1 \\ -1 & -1 & 2 \end{bmatrix} \begin{bmatrix} S_1 \\ S_3 \\ S_5 \end{bmatrix} \tag{1}$$

where switch position $S_j \in \{0,1\}$.

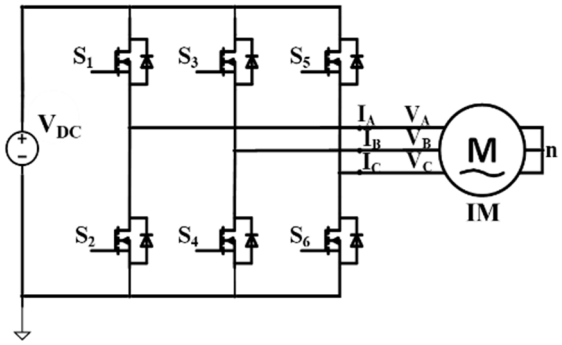

Fig. 2. A voltage-source inverter connected to IM

B. Dynamic Model of Induction Motor

In this study, the dynamic model of the IM in rotor flux orientation is used. Park transformations are applied to three-phase stator currents, and the *d-q* axis stator currents are given in (2)-(3) [30].

$$\begin{aligned} \frac{di_{sd}}{dt} = &-\frac{L_r R_s + L_m^2/\tau_r}{\sigma L_s L_r} i_{sd} + \omega_g i_{sq} \\ &+ \frac{L_m}{\tau_r \sigma L_s L_r} \psi_{rd} + \frac{v_{sd}}{\sigma L_s} \\ &+ \frac{L_m}{\sigma L_s L_r} \omega_e \psi_{rq} \end{aligned} \tag{2}$$

$$\begin{aligned} \frac{di_{sq}}{dt} = &-\frac{L_r R_s + L_m^2/\tau_r}{\sigma L_s L_r} i_{sq} - \omega_g i_{sd} \\ &+ \frac{L_m}{\tau_r \sigma L_s L_r} \psi_{rq} + \frac{v_{sq}}{\sigma L_s} \\ &- \frac{L_m}{\sigma L_s L_r} \omega_e \psi_{rd} \end{aligned} \tag{3}$$

where v_{sd}, v_{sq} are *d-q* axis stator voltages, i_{sd}, i_{sq} are *dq-* axis currets, ψ_{rd}, ψ_{rq} are *d-q* axis rotor fluxes, L_s, L_r, L_m are stator, rotor and mutual inductances respectively, $\tau_r = L_r/R_r$ is rotor time constant, $\sigma = (L_r L_s - L_m^2)/L_r L_s$ is leakage constant, ω_g is synchronous angular speed, $\omega_e = P\omega_m$ is electrical angular speed where P is the machine pole pair number, and ω_m is mechanical angular speed. The dynamic expressions of rotor fluxes with respect to *d-q* axis are given in (4)-(5), and electromagnetic torque expression is given in (6).

$$\frac{d\psi_{rd}}{dt} = \frac{L_m}{\tau_r} i_{sd} - \frac{\psi_{rd}}{\tau_r} + (\omega_g - \omega_e)\psi_{rq} \tag{4}$$

$$\frac{d\psi_{rq}}{dt} = \frac{L_m}{\tau_r} i_{sq} - \frac{\psi_{rq}}{\tau_r} - (\omega_g - \omega_e)\psi_{rd} \tag{5}$$

$$T_e = \frac{3P}{2}\frac{L_m}{L_r}(\psi_{rd} i_{sq} - \psi_{rq} i_{sd}) \tag{6}$$

In rotor flux orientation, the magnitude of the rotor flux vector is aligned with the *d*-axis rotor flux. This gives $\psi_{rq} = d\psi_{rq}/dt = 0$ in steady-state. The slip angular speed can be found by writing this term into (5) [30].

$$\omega_{sl} = \omega_g - \omega_e = \frac{L_m}{\tau_r \psi_{rd}} i_{sq} \tag{7}$$

By writing the $\psi_{rq} = d\psi_{rq}/dt = 0$ into (4), field-orientation is completed. This way, the rotor flux value becomes proportional to the *d*-axis current, as given in (8). Thus, the flux desired to be produced in the rotor can be controlled by i_{sd}.

$$i_{sd} = \frac{\psi_{rd}}{L_m} \tag{8}$$

Electromagnetic torque expression given in (6) becomes as given in (9) with the completion of rotor flux orientation. Thus, electromagnetic torque becomes proportional to *q*- axis. Using rotor flux orientation, IM can be controlled as a seperatly-exicted direct current (DC) motor.

$$T_e = K_t i_{sq} \tag{9}$$

$K_t = \frac{3P}{2}\frac{L_m \psi_{rd}}{L_r}$ is the torque constant. Thus, the electromagnetic torque of IM can be controlled by i_{sq}. In the next section, the operating logic and the mathematical expressions of the TD3 agent will be given.

III. Fundamentals of TD3 Agent

TD3 is one of the deep RL methods, an extension of the DDPG agent. DDPG and TD3 agents are actor-critic-based agents. Because they are director-critic based, these agents can handle continuous-action problems that other RL agents, such as DQN, cannot [31]. In order to give mathematical expressions of TD3, the mathematical expressions of the DQN agent must first be given. DQN agent is a critic-based agent-based on the Bellman equation given in (10) [25].

$$g_k = q(o_k, a_k) = E\{R_{k+1} + \gamma q(O_{k+1}, A_{k+1}) \mid O_k = o_k, A_k = a_k\} \tag{10}$$

The Bellman equation gives the possible Q value of acting an action in an environment. Using neural networks, the DQN agent selects the action that offers the maximum Q value and applies it to the environment. For the neural network to learn, the weights of the neural network must be updated. For this reason, the weights of the created neural network, which $\widehat{q_\theta}$ represents the neural network, and θ represents the weights of the neural network, which is updated using the so-called loss function, which is the mean squared error minimization problem given in (11) [32].

$$L_Q = \frac{1}{|B|}\sum_{k=1}^{B}\left(\left(R_{k+1} + \gamma \max_{a_{k+1}} \widehat{q_{\theta,target}}(o_{k+1}, a_{k+1})\right) - \widehat{q_\theta}(o_k, a_k)\right)^2 \tag{11}$$

where B is the mini-batch size. $\widehat{q_{\theta,target}}$ is the target neural network and it is the same with $\widehat{q_\theta}$. The critic networks of DDPG and TD3 agents are the same as the DQN agent. However, while the DDPG agent uses a single critic network, the TD3 agent uses a double critic network. Thus, by choosing the smaller Q value, the overestimation problem in the DDPG agent is solved [33]. In the TD3 agent, the actor uses the policy gradient approach to create a policy that consists of continuous actions. The policy gradient approach is given in (12)-(13) [34].

$$\nabla_{\theta^\pi} J(\pi) = E\left[\nabla_a Q(o_k, a_k|\theta^Q)|_{a=\pi(o_k)} \cdot \nabla_{\theta^\pi}\pi(o_k|\theta^\pi)\right] \tag{12}$$

$$J_{k+1} = J_k - \eta \nabla J_k \tag{13}$$

where η is the learning rate. Then, the critic network uses the temporal difference approach to calculate the value of the policy created by the actor. Weight updates for the actor target network and critic target network can be done using (15)-(16) [35].

$$\theta^{\pi_{target}} \leftarrow (1-\rho)\theta^{\pi_{target}} + \rho\theta^\pi \tag{14}$$

$$\theta^{Q_{target}} \leftarrow (1-\rho)\theta^{Q_{target}} + \rho\theta^Q \tag{15}$$

where ρ is the target smoothing factor. The same mathematical expression given in DQN is used to update the critic network in TD3. The actor-network modifies the policy based on the value the critic network determines. The agent selects the optimum action that maximizes the cumulative reward. Then, this action is applied to the environment. Fig. 3 shows the designed TD3 agent-based drive system. As can be seen in Figure 3, the inner control loop is the TD3 agent, and the outer control loop is the PI controller. The observation vector, which consists of the signals that the agent interacts with the environment, is chosen as given in (16). Due to the nature of neural networks, normalization must be applied to these signals.

$$o_k = \left[I_{d_{ref}}, I_{q_{ref}}, I_d, I_q, I_{d_{error}}, I_{q_{error}}, \omega_{ref}, \omega_m\right] \tag{16}$$

As the agent interacts with the environment using (16), it creates a policy consisting of actions that maximize the reward function given in (17). The reward function is designed similarly to the cost function in the FCS-MPC technique.

$$R_k = -\left(C_1\left|I_{d,ref} - I_d\right|^2 + C_2\left|I_{q,ref} - I_q\right|^2 + C_3 a_{k-1}\right) \tag{17}$$

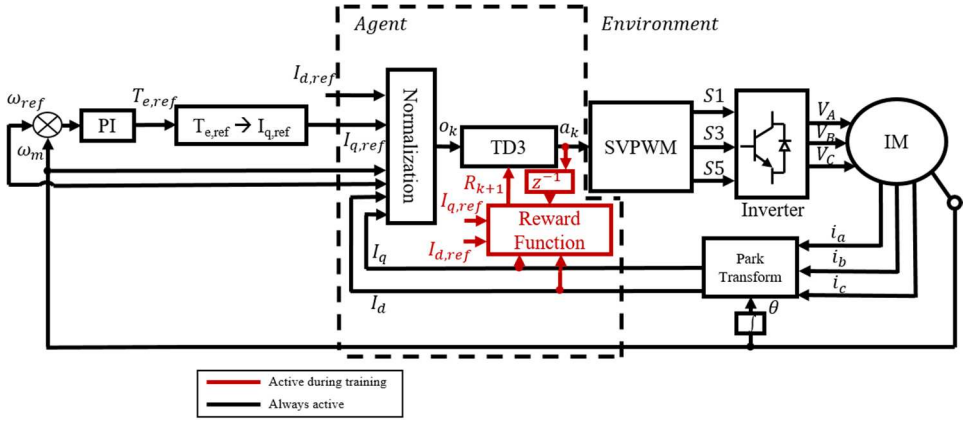

Fig. 3. Block diagram of the designed control system

Reference *d-q* axis voltages were selected as the action to be taken by the agent. The optimum switching vectors are generated using the SVPWM technique and applied to the switches in the inverter. Thus, the reference voltage value produced at the output of the TD3 agent is produced in the machine.

IV. Simulation Results

The speed control of IM using the TD3 agent is performed in a Matlab© environment. First, the simulation results of controlling IM with the TD3 agent, whose parameters have been changed, are given. Then, the dynamic and steady-state results of the agent are compared with FOC, FCS-MPC, and M^{2}PC techniques. The simulation parameters are presented in Table I.

Table I. Simulation Parameters

Parameter	Description	Values
V_{DC}	DC bus voltage	150 V
P	Number of pole pairs	2
T_e	Nominal torque	7.5 Nm
L_m	Mutual inductance	442.3 mH
L_{ls}	Stator leakage inductance	10.145 mH
L_{lr}	Rotor leakage inductance	10.061 mH
R_s	Stator resistance	3.919 Ω
R_r	Rotor resistance	4.9618 Ω
T_s	Sampling time	100 µs
B	Mini-batch size	512
D	Buffer length	2×10^6
γ	Discount factor	0.995
ρ	Target smoothing factor	0.005
η	Learn rate	1×10^{-3}
K	Number of episodes	1500

The simulation time is set to t=6 s, and the simulation scenarios are the same for all simulations. At t=0-1.5 s, the reference speed is set to ω_{ref}=300 rpm, and the load torque is set to T_L=1.5 Nm. During this period, the parameters of the machine are kept at their nominal values, as given in Table 1. At t=1.5 s, the reference speed of the machine is increased to ω_{ref}=500 rpm. Thus, the performance of the control system to the step increase in speed is examined. Considering that the temperature of the motor is increased at t=2.5 s, the rotor resistance (R_r) is reduced by %50 from its nominal value by using a step function [36]. At t=4 s, the load torque is increased to T_L=2.5 Nm. Thus, the response of the system to the load step is examined. As a result of magnetic saturation at t=5 s, the mutual inductance (L_m) is increased by %30 from its nominal value using the step function [36]. The simulation results are shown in Figure 4.

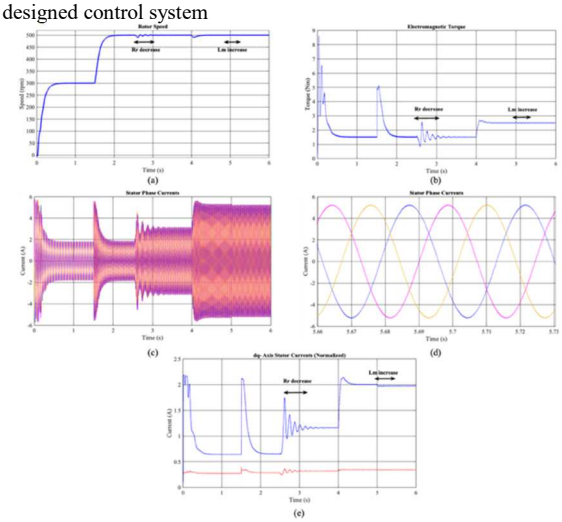

Fig. 4. Results of the designed control system: a) Rotor speed, b) Electromagnetic torque, c) Phase currents, d) Zoom-in phase currents, e) Normalized d-q axis currents

As can be seen in Figure 4, the control system reaches the reference speed value of ω_{ref}=300 rpm in ~0.5 s, without any unwanted undershoot or overshoot at the start-up. As the outer PI controller adjusts the loading torque as a result of the speed error, the electromagnetic torque produced by the machine is equal to the load torque of T_L=1.5 Nm in ~0.5 s, and then the system becomes steady-state. When speed step increase is demanded at t=1.5 s, the TD3 agent increases the frequencies of the phase currents, and the system reaches the new reference speed value of ω_{ref}=500 rpm in ~0.5 s without overshoot and undershoot. At t=2.5 s, due to the decrease in R_r due to the temperature increase of the machine, there is an oscillation in speed and, therefore, in torque. After an undershoot of ~10 rpm, the agent increases the magnitude of the phase currents, and the system becomes steady-state in ~0.35 s. As a result of the step increase in the load torque at t=4 s, there is a ~9 rpm decrease in the speed of the machine. However, by adjusting the new reference torque value, the outer loop PI controller quickly reacts to the decrease. Then, the TD3 agent adjusts the current magnitudes according to this new reference torque value of T_L=2.5 Nm. Due to the increase in L_m at t=5 s, there are very small oscillations in the speed and electromagnetic torque of the system that would not affect the system. *d-q* axis reference currents that change depending on this increase in the system. The *d*- axis current increased, and the *q*- axis current decreased due to this increase. Overall, the designed control system with TD3 agent is robust against parameter changes, and the dynamic and steady-state performance of the system is good against step changes in load

torque and speed. The performance of the control system designed with the TD3 agent is compared with FOC, FCS-MPC, and M^{2}PC techniques in terms of speed, electromagnetic torque, stator phase A current magnitude, and total harmonic distortion (THD) as given in Figure 5, Table 2 and Table 3, respectively. The sampling time of FCS-MPC is chosen as T_s=50 µs, and for other techniques, the sampling time is selected as Ts=100 µs.

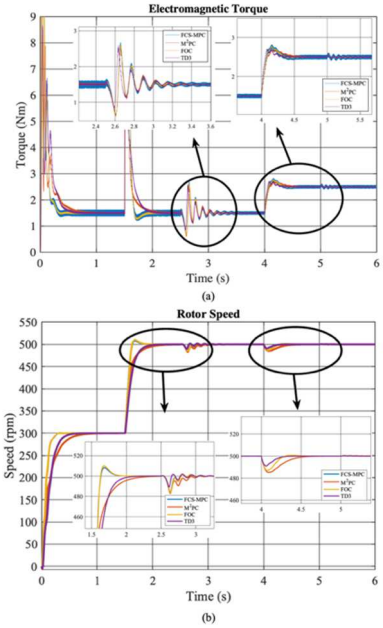

Fig. 5. Performance comparison of different control techniques; a) Electromagnetic torque, b) Rotor speed

As shown in Figure 5, there is no unwanted overshoot or undershoot in any of the speed responses of the control techniques at the start-up. The settling times of FCS-MPC and FOC techniques are the fastest and closest to each other. Next comes the TD3 agent with a difference of ~0.3 s, and finally, the M^{2}PC technique. The same comment is made for the electromagnetic torque responses of control systems at the start-up. When the reference speed is increased to ω_{ref}=500 rpm, it can be seen that there is a ~10 rpm overshoot in the speed responses of the control systems with FCS-MPC and FOC techniques. Also, there is an undershoot in the electromagnetic torque responses of these control systems. There is no overshoot or undershoot in the speed and torque responses of control systems with the TD3 agent and M^{2}PC technique. The settling time of the control system designed with the TD3 agent is ~0.3 s slower than the control systems with FOC and FCS-MPC techniques. However, as an advantage, there is no unwanted undershoot or overshoot in the speed and electromagnetic torque responses of the control system designed with the TD3 agent. When R_r is decreased depending on temperature, it can be seen in Figure 5 that the control system with the lowest overshoot-undershoot and fastest response is the control system designed with the TD3 agent. When the load torque increased to T_L=2.5 Nm, the system with the lowest undershoot in speed response is the control system with the TD3 agent. In addition, the control system with the TD3 agent shows the fastest response in speed and electromagnetic torque responses. In control systems with FOC and FCS-MPC techniques, it can be seen that there is undershoot and overshoot in the speed responses when the load torque is increased. When L_m is increased depending on the magnetic saturation, the responses of the control systems are almost the same. When comparing the THD of control techniques, it is necessary to look at Table 2 and the current magnitudes of the stator phase A given in Table 3. It can be seen from Table 2 and Table 3, the current drawn by the machine in the control system with TD3 agent is lower than other techniques. Also, at both electromagnetic torque values, the phase A current THD value of the TD3 agent is only %0.02 greater than the M^{2}PC technique. At the same current magnitudes, one can say that the THD value of the TD3 agent will be lower than other techniques. The TD3 agent draws lower current at the same electromagnetic torque values, making the control system more efficient than other techniques. Overall, the control system designed with TD3 agent shows better performance in dynamic and steady-state than other techniques.

Table II. Comparison Results in terms of THD

Electromagnetic Torque / **Control Technique**	**1.5 Nm (t=3.8 s)**	**2.5 Nm (t=5.8 s)**
FCS-MPC	%2.25	%1.32
M^{2}PC	%0.58	%0.39
FOC	%0.58	%0.5
TD3	%0.6	%0.41

Table III. Comparison Results in terms of magnitude of Phase Current A

Electromagnetic Torque / **Control Technique**	**1.5 Nm (t=3.8 s)**	**2.5 Nm (t=5.8 s)**
FCS-MPC	3.28 A	5.45 A
M^{2}PC	3.265 A	5.42 A
FOC	3.27 A	5.42 A
TD3	3.125 A	5.22 A

V. CONCLUSION

In this study, firstly, the dynamic and steady-state control performances of the TD3 agent against varying machine parameters were examined. Secondly, the control performance when the machine parameters vary of the TD3 agent was compared with FOC, FCS-MPC, and M^{2}PC. Extensive simulation results have shown that the control system designed with the TD3 agent was robust according to varying machine parameters. Also, it has been shown that the dynamic and steady-state performance of the TD3 agent was more robust than other control techniques, that it did not cause any undesirable overshoots and undershoots, and that the system response was faster. In summary, the dynamic and steady-state performance of the TD3 agent-based controller is better than the other techniques. Moreover, the machine draws a lower current in the control system with the TD3 agent; thus, it is evident that the control system is more efficient than the other techniques.

REFERENCES

[1] C. M. Verrelli, A. Savoia, M. Mengoni, R. Marino, P. Tomei, and L. Zarri, "On-line identification of winding resistances and load torque in induction machines," *IEEE Transactions on Control Systems Technology*, vol. 22, no. 4, pp. 1629–1637, 2014, doi: 10.1109/TCST.2013.2285604.

[2] G. Ozkurt and E. Zerdali, "Design and Implementation of Hybrid Adaptive Extended Kalman Filter for State Estimation of Induction Motor," *IEEE Trans Instrum Meas*, vol. 71, 2022, doi: 10.1109/TIM.2022.3144729.

[3] M. Wu, X. Sun, J. Zhu, G. Lei, and Y. Guo, "Improved Model Predictive Torque Control for PMSM Drives Based on Duty Cycle Optimization," *IEEE Trans Magn*, vol. 57, no. 2, 2021, doi: 10.1109/TMAG.2020.3008495.

[4] B. GÖRDÜK, "DESING AND IMPLEMENTATION OF SENSORLESS VECTOR CONTROLLED DRIVE FOR PMSMs," Istanbul Technical University, Electrical Engineering, Istanbul, 2019.

[5] I. Takahashi and T. Noguchi, "A New Quick-Response and High-Efficiency Control Strategy of an Induction Motor," *IEEE Trans Ind Appl*, vol. IA-22, no. 5, pp. 820–827, 1986, doi: 10.1109/TIA.1986.4504799.

[6] J. Tang, Y. Yang, F. Blaabjerg, J. Chen, L. Diao, and Z. Liu, "Parameter identification of inverter-fed induction motors: A review," *Energies (Basel)*, vol. 11, no. 9, pp. 1–21, 2018, doi: 10.3390/en11092194.

[7] Y. Hu, T. K. Chau, X. Zhang, H. H. C. Iu, T. Fernando, and D. Fan, "A Novel Adaptive Model Predictive Control Strategy for DFIG Wind Turbine With Parameter Variations in Complex Power Systems," *IEEE Transactions on Power Systems*, vol. 38, no. 5, pp. 4582–4592, 2023, doi: 10.1109/TPWRS.2022.3213085.

[8] S. Dwivedi, S. M. Tripathi, and S. K. Sinha, "Review on Control Strategies of Permanent Magnet-Assisted Synchronous Reluctance Motor Drive," in *2020 International Conference on Power Electronics and IoT Applications in Renewable Energy and its Control, PARC 2020*, 2020, pp. 124–128. doi: 10.1109/PARC49193.2020.236570.

[9] H. Mohan, M. K. Pathak, and S. K. Dwivedi, "Direct power control of induction motor drives," *Proceedings - 2019 IEEE 13th International Conference on Compatibility, Power Electronics and Power Engineering, CPE-POWERENG 2019*, pp. 1–5, 2019, doi: 10.1109/CPE.2019.8862412.

[10] F. Wang, Z. Zhang, X. Mei, J. Rodríguez, and R. Kennel, "Advanced control strategies of induction machine: Field oriented control, direct torque control and model predictive control," *Energies (Basel)*, vol. 11, no. 1, 2018, doi: 10.3390/en11010120.

[11] M. Gokdag, "Modulated Predictive Control to Improve the Steady-State Performance of NSI-Based Electrification Systems," *Energies (Basel)*, vol. 15, no. 6, 2022, doi: 10.3390/en15062043.

[12] H. Xie *et al.*, "Cooperative Decision-Making Approach for Multiobjective Finite Control Set Model Predictive Control Without Weighting Parameters," *IEEE Transactions on Industrial Electronics*, vol. 71, no. 5, pp. 4495–4506, May 2024, doi: 10.1109/TIE.2023.3283689.

[13] J. P. Zucuni, F. Carnielutti, H. Pinheiro, M. Norambuena, and J. Rodriguez, "Cost Function Design for Stability Assessment of Modulated Model Predictive Control," in *2020 22nd European Conference on Power Electronics and Applications, EPE 2020 ECCE Europe*, Lyon, France: IEEE, 2020, pp. 1–9. doi: 10.23919/EPE20ECCEEurope43536.2020.9215797.

[14] U. U. Korpe, M. Gokdag, M. Koc, and O. Gulbudak, "Modulated Model Predictive Control of Permanent Magnet Synchronous Motors with Improved Steady-State Performance," in *Proceedings - 2021 IEEE 3rd Global Power, Energy and Communication Conference, GPECOM 2021*, Antalya, Turkey: IEEE, 2021, pp. 67–72. doi: 10.1109/GPECOM52585.2021.9587747.

[15] X. Gao *et al.*, "Modulated Model Predictive Control of Modular Multilevel Converters Operating in a Wide Frequency Range," *IEEE Transactions on Industrial Electronics*, vol. 70, no. 5, pp. 4380–4391, May 2023, doi: 10.1109/TIE.2022.3183354.

[16] J. Andino, P. Ayala, J. Llanos-Proano, D. Naunay, W. Martinez, and D. Arcos-Aviles, "Constrained Modulated Model Predictive Control for a Three-Phase Three-Level Voltage Source Inverter," *IEEE Access*, vol. 10, pp. 10673–10687, 2022, doi: 10.1109/ACCESS.2022.3144669.

[17] L. Broghammer *et al.*, "Reinforcement Learning Control of Six-Phase Permanent Magnet Synchronous Machines," in *2023 13th International Electric Drives Production Conference, EDPC 2023 - Proceedings*, Institute of Electrical and Electronics Engineers Inc., 2023. doi: 10.1109/EDPC60603.2023.10372153.

[18] D. Jakobeit, M. Schenke, and O. Wallscheid, "Meta-Reinforcement-Learning-Based Current Control of Permanent Magnet Synchronous Motor Drives for a Wide Range of Power Classes," *IEEE Trans Power Electron*, vol. 38, no. 7, pp. 8062–8074, Jul. 2023, doi: 10.1109/TPEL.2023.3256424.

[19] Z. Tir, T. Orlowska-Kowalska, H. Ahmed, and A. Houari, "Adaptive High Gain Observer Based MRAS for Sensorless Induction Motor Drives," *IEEE Transactions on Industrial Electronics*, vol. 71, no. 1, pp. 271–281, 2024, doi: 10.1109/TIE.2023.3243271.

[20] A. Dianov and A. Anuchin, "Offline Measurement of Stator Resistance and Inverter Voltage Drop Using Least Squares," *IEEE Access*, vol. 11, no. January, pp. 17053–17065, 2023, doi: 10.1109/ACCESS.2023.3245663.

[21] M. Nachtsheim, J. Ernst, C. Endisch, and R. Kennel, "Performance of Recursive Least Squares Algorithm Configurations for Online Parameter Identification of Induction Machines in an Automotive Environment," *IEEE Transactions on Transportation Electrification*, vol. 9, no. 3, pp. 4236–4254, Sep. 2023, doi: 10.1109/TTE.2023.3244619.

[22] S. Zhang, O. Wallscheid, and M. Porrmann, "Machine Learning for the Control and Monitoring of Electric Machine Drives: Advances and Trends," *IEEE Open Journal of Industry Applications*, vol. 4, pp. 188–214, 2023, doi: 10.1109/OJIA.2023.3284717.

[23] T. Schindler, L. Broghammer, P. Karamanakos, A. Dietz, and R. Kennel, "Deep Reinforcement Learning Current Control of Permanent Magnet Synchronous Machines," in *2023 IEEE International Electric Machines and Drives Conference, IEMDC 2023*, Institute of Electrical and Electronics Engineers Inc., 2023. doi: 10.1109/IEMDC55163.2023.10238988.

[24] M. Schenke, W. Kirchgassner, and O. Wallscheid, "Controller Design for Electrical Drives by Deep Reinforcement Learning: A Proof of Concept," *IEEE Trans Industr Inform*, vol. 16, no. 7, pp. 4650–4658, Jul. 2020, doi: 10.1109/TII.2019.2948387.

[25] M. Schenke and O. Wallscheid, "A Deep Q-Learning Direct Torque Controller for Permanent Magnet Synchronous Motors," *IEEE Open Journal of the Industrial Electronics Society*, vol. 2, pp. 388–400, 2021, doi: 10.1109/OJIES.2021.3075521.

[26] Ayesha and A. Y. Memon, "Reinforcement Learning Based Field Oriented Control Of An Induction Motor," in *Proceedings of 3rd International Conference on Latest Trends in Electrical Engineering and Computing Technologies, INTELLECT 2022*, Institute of Electrical and Electronics Engineers Inc., 2022. doi: 10.1109/INTELLECT55495.2022.9969403.

[27] F. Yin, X. Yuan, Z. Ma, and X. Xu, "Vector Control of PMSM Using TD3 Reinforcement Learning Algorithm," *Algorithms*, vol. 16, no. 9, Sep. 2023, doi: 10.3390/a16090404.

[28] G. Book *et al.*, "Transferring online reinforcement learning for electric motor control from simulation to real-world experiments," *IEEE Open Journal of Power Electronics*, vol. 2, pp. 187–201, 2021, doi: 10.1109/OJPEL.2021.3065877.

[29] J. Rodríguez *et al.*, "Predictive Current Control of a Voltage Source Inverter," *IEEE Transactions on Industrial Electronics*, vol. 54, no. 1, pp. 495–503, 2007, doi: 10.1109/TIE.2006.888802.

[30] M. Gokdag and O. Gulbudak, "Dual-model predictive control of two independent induction motors driven by a SiC nine-switch inverter," *International Journal of Electronics*, vol. 00, no. 00, pp. 1–19, 2021, doi: 10.1080/00207217.2021.2007545.

[31] J. Ruan, C. Wu, H. Cui, W. Li, and D. U. Sauer, "Delayed Deep Deterministic Policy Gradient-Based Energy Management Strategy for Overall Energy Consumption Optimization of Dual Motor Electrified Powertrain," *IEEE Trans Veh Technol*, vol. 72, no. 9, pp. 11415–11427, Sep. 2023, doi: 10.1109/TVT.2023.3265073.

[32] B. Haucke-Korber, M. Schenke, and O. Wallscheid, "Deep Q Direct Torque Control with a Reduced Control Set Towards Six-Step Operation of Permanent Magnet Synchronous Motors," in *2023 IEEE International Electric Machines and Drives Conference, IEMDC 2023*, Institute of Electrical and Electronics Engineers Inc., 2023. doi: 10.1109/IEMDC55163.2023.10239018.

[33] F. Yin, X. Yuan, Z. Ma, and X. Xu, "Vector Control of PMSM Using TD3 Reinforcement Learning Algorithm," *Algorithms*, vol. 16, no. 9, Sep. 2023, doi: 10.3390/a16090404.

[34] X. Qi, W. Cao, and L. Aarniovuori, "Reinforcement Learning Based Parameter Lookup Table Generating Method for Optimal Torque Control of Induction Motors," *IEEE Transactions on Industrial Electronics*, vol. 70, no. 5, pp. 4516–4525, May 2023, doi: 10.1109/TIE.2022.3189103.

[35] Y. Wang, S. Fang, and D. Huang, "An Improved Model-Free Active Disturbance Rejection Deadbeat Predictive Current Control Method of PMSM Based on Data-Driven," *IEEE Trans Power Electron*, vol. 38, no. 8, pp. 9606–9616, Aug. 2023, doi: 10.1109/TPEL.2023.3280013.

[36] S. Yang, D. Ding, X. Li, Z. Xie, X. Zhang, and L. Chang, "A Novel Online Parameter Estimation Method for Indirect Field Oriented Induction Motor Drives," *IEEE Transactions on Energy Conversion*, vol. 32, no. 4, pp. 1562–1573, Dec. 2017, doi: 10.1109/TEC.2017.2699681.